A model analysis of climate and CO2 controls on tree growth and carbon allocation in a semi-arid woodland

A model analysis of climate and CO_2 controls on tree growth and carbon allocation in a semi-arid woodland

Guangqi Li[1,2], Sandy P. Harrison[1,2] and I. Colin Prentice[1,3]

1 Department of Biological Sciences, Macquarie University, North Ryde, NSW 2109, Australia

2 School of Archaeology, Geography and Environmental Sciences (SAGES), Reading University, Reading, UK

3 AXA Chair of Biosphere and Climate Impacts, Imperial College London, Silwood Park Campus, Buckhurst Road, Ascot SL5 7PY, UK

Correspondence to: G. Li (g.li2@reading.ac.uk)

Abstract

Many studies have failed to show an increase in the radial growth of trees in response to increasing atmospheric CO_2 concentration [CO_2] despite the expected enhancement of photosynthetic rates and water-use efficiency at high [CO_2]. A global light use efficiency model of photosynthesis, coupled with a generic carbon allocation and tree-growth model based on mass balance and tree geometry principals, was used to simulate annual ring-width variations for the gymnosperm *Callitris columellaris* in the semi-arid Great Western Woodlands, Western Australia, over the past 100 years. Parameter values for the tree-growth model were derived from independent observations except for sapwood specific

respiration rate, fine-root turnover time, fine-root specific respiration rate and the ratio of fine-root mass to foliage area (ζ), which were calibrated to the ring-width measurements by approximate Bayesian calibration. This procedure imposed a strong constraint on ζ. Modelled and observed ring-widths showed quantitatively similar, positive responses to total annual photosynthetically active radiation and soil moisture, and similar negative responses to vapour pressure deficit. The model also produced enhanced radial growth in response to increasing [CO_2] during recent decades, but the data do not show this. Recalibration in moving 30-year time windows produced temporal shifts in the estimated values of ζ, including an increase by *ca* 12% since the 1960s, and eliminated the [CO_2]-induced increase in radial growth. The potential effect of CO_2 on ring-width was thus shown to be small compared to effects of climate variability even in this semi-arid climate. It could be counteracted in the model by a modest allocation shift, as has been observed in field experiments with raised [CO_2].

Keywords

Tree growth modelling, Tree rings, CO_2 fertilisation, Carbon allocation, Response to climate change, Water-use efficiency.

Introduction

Atmospheric CO_2 concentration [CO_2] has direct impacts on the photosynthesis and water-use efficiency of C_3 plants (Drake et al., 1997; Ainsworth and Long, 2005; Norby and Zak, 2011; De Kauwe et al., 2013). However, several studies of tree radial growth in well-watered temperate and tropical regions have failed to show increases that might be attributed to increasing [CO_2] (Kienast and Luxmoore, 1988; Gedalof and Berg, 2010;

47 Girardin et al., 2011; Peñuelas et al., 2011; van der Sleen et al., 2015). Moreover, tree-
48 growth modelling (Boucher et al., 2014; Li et al., 2014) has suggested that the expected
49 radial growth enhancement due to the recent [CO_2] increase is quite small, compared to the
50 effects of climate variability. A stronger response to enhanced [CO_2] might be expected *a*
51 *priori* in water-limited regions (Field et al., 1983; Hyvönen et al., 2007), because stomatal
52 conductance is reduced when [CO_2] is higher. This is a common empirical observation,
53 consistent with the least-cost hypothesis (Wright et al., 2003; Prentice et al., 2014), which
54 predicts a near-constant ratio of leaf-internal to ambient [CO_2] as [CO_2] increases – while
55 the rate of increase of photosynthesis with [CO_2] declines. Failure to sample water-limited
56 environments might thus conceivably explain the apparent lack of increased stem growth in
57 response to increasing [CO_2].

58

59 An alternative explanation could be that increased primary production due to increased
60 [CO_2] has not led to increased stem growth due to a shift in carbon allocation away from
61 stems. There is some experimental evidence that changing [CO_2] results in changes in
62 carbon allocation between above-ground (leaf, stem) and below-ground (root) biomass
63 pools. Observations of the response to high [CO_2] in Free-Air Carbon dioxide Enrichment
64 (FACE) experiments show that trees commonly increase total carbon allocation below
65 ground, in the form of increased root production and/or exudation of labile substrates (Oak
66 Ridge FACE: Norby et al., 2004; DUKE-FACE: DeLucia et al., 1999; Pritchard et al., 2008;
67 Rhinelander ASPEN-FACE: King et al., 2001; EUROFACE: Calfapietra et al., 2003; Lukac
68 et al., 2003; Bangor FACE: Smith et al., 2013). In some sites, this increase is clearly at the
69 expense of stem growth (Battipaglia et al., 2013). However, monitoring of below-ground
70 carbon dynamics is challenging and there are no direct, long-term observations of the
71 response of below-ground allocation to gradually increasing [CO_2] under natural conditions.

Process-based model experiments provide a way of comparing the consequences of alternative hypotheses. Here we used a global light-use efficiency model of photosynthesis coupled with a dynamic allocation and tree-growth model to simulate the radial growth of the gymnosperm *Callitris columellaris* growing in the water-limited environment of the Great Western Woodlands (GWW), Western Australia. We specifically examined whether we could detect an effect of [CO_2] on ring-width, in addition to effects of climate variability.

2 Methods

2.1 The study area

The GWW, with an area of about 160,000 km^2, is the largest remaining area of intact mediterranean woodland on Earth (Watson, 2008; Lee et al., 2013). The region is unique because of the abundance and diversity of trees that grow there, despite the dry climate and nutrient-poor sandy soils (Watson, 2008; Prober et al., 2012). The vegetation of the GWW is dominated by open eucalypt woodlands, with patches of heathland, mallee and grassland. The climate is characterized by winter rainfall and summer drought, although storms associated with monsoonal penetration into the continental interior can also bring occasional heavy rains in summer (Sturman and Tapper, 1996). The sampling site lies near the GWW SuperSite (GWW SuperSite, Credo, 30.1°S, 120.7°E, 400m a.s.l.; http://www.tern-supersites.net.au/supersites/gwwl) in the northernmost and driest part of the GWW, with a mean annual rainfall *ca* 270 mm. The area around the GWW SuperSite is dominated by naturally regenerating eucalypts (*Eucalyptus salmonophloia* and *E. salubris*),

96 associated with *Acacia* and the multi-stemmed gymnosperm *Callitris columellaris*, with
97 *Atriplex* in the understory. However, *Callitris columellaris* was the only woody species at the
98 sampling site itself. Human impact around the site is minimal.

99

100 The coastal southwestern region of Western Australia has experienced a multidecadal
101 drought that began in the mid-1970s (Ansell et al., 2000; Cai and Cowan, 2006; Hope et al.,
102 2006; Cullen and Grierson, 2009; Van Ommen and Morgan, 2010), characterized by a large
103 reduction in winter rainfall. The CRU TS v3.22 climate data (Harris et al., 2014) for the
104 GWW show abruptly reduced winter rainfall from around 1990 but total annual precipitation
105 has increased, by about 7 mm/decade over the century (p = 0.015), due to enhanced
106 summer storms. The number of rain days decreased, especially after 1960 (–6.2
107 day/decade, p < 0.001) while the mean precipitation on rain days (precipitation intensity)
108 increased (0.38 mm/decade, p < 0.001). These trends are superimposed on large
109 interannual variability, with annual rainfall ranging from *ca* 100 to > 400 mm. Mean annual
110 temperature increased by 0.16˚/decade (p < 0.001) and vapour pressure deficit (VPD) also
111 increased, while soil moisture (as indexed by α, the ratio of modelled actual to potential
112 evapotranspiration: Cramer and Prentice, 1988) showed an initially increasing trend that
113 flattened off after 1960.

114

115 **2.2 Tree ring data**

116 The genus *Callitris* has provided good records of annual tree growth in a variety of climates
117 across Australia and is known to be sensitive to changing water availability (Ash, 1983;
118 Cullen and Grierson, 2007; Baker et al., 2008; Cullen et al., 2008; Cullen and Grierson,
119 2009). We selected a 500 x 500 m plot near the GWW SuperSite, where *Callitris*

120 *columellaris was* the only woody species present, for sampling. Although the basic
121 measurements required to characterize tree growth (see 2.4) were made on all the trees in
122 the plot (146 individuals), tree-ring cores were obtained from only ten of these trees (Fig. 1).
123 The sampling was carried out in August 2013. The selected trees were canopy trees, with a
124 mean height of 4.2 meters, not overshadowed by other individuals, and were chosen
125 because they appeared to be the oldest trees on the plot. The sampling plot showed no
126 sign of disturbance. Other environmental conditions (topography, soil type, soil depth)
127 showed no visible variation among the sampled trees. Multiple cores were obtained from
128 each tree, taking care to sample each of the individual stems of each tree. A total of 32 tree
129 ring cores were obtained.

130

131 Annual growth was measured on each core. The cores were cross-dated visually, based on
132 pointing-year identification and ring-width pattern matching, and the final measuring
133 accuracy was checked with the cross-dating software COFECHA (Holmes, 1983). The
134 measurements of tree growth on individual stems were aggregated to produce an estimate
135 of the total radial growth of each tree for comparison with model outputs. The "effective"
136 single-stemmed basal diameter (D) and "effective" single-stemmed diameter increment
137 (dD/dt) were obtained from observed multi-stemmed basal diameter (δ_i) and individual-stem
138 diameter increments ($d(\delta_i)/dt$) by:

139 $D = \sqrt{\sum_{i=1}^{n} \delta_i^2}$, and $dD/dt = \frac{1}{D}\sum_{i=1}^{n}(\delta_i \cdot d\delta_i/dt)$

140 The effective annual growth measured at the site is shown in Fig. 1. Note that, in contrast
141 with traditional tree-ring studies, the ring-width series were not detrended to account for
142 ageing because ageing effects are explicitly simulated by our model.. Furthermore, we
143 simulate each of the ten sampled trees individually rather than creating a composite series.

144 Nevertheless, there is reasonable coherency between the records from the individual cores
145 and individual trees (Table 1).

146

147 Tree-ring series from the Southern Hemisphere are conventionally presented with annual
148 increments attributed to the calendar year in which tree growth was initiated (Schulman,
149 1956). Although the longest record obtained dates from 1870 (Fig. 1), only three trees have
150 pre-1920 records. Some early changes such as the step-like decrease and increase before
151 1920 are likely to be artifacts because of the small number of long records. For this reason,
152 and because the climate data are also less reliable in the early decades of the 20th century,
153 we focus our analysis on the years since 1920.

154

155 **2.3 The tree-growth model**

156 We used a generic light-use efficiency model (the P model, Wang et al., 2014) to simulate
157 gross primary production (GPP). Wang et al. (2014) demonstrated the model's ability to
158 reproduce global geographic and seasonal patterns in GPP derived from flux
159 measurements. Potential GPP (the GPP that would be predicted if all incident PAR were
160 absorbed) is calculated in the model from latitude, elevation, [CO_2], and monthly
161 temperature, precipitation, and fractional cloud cover. It depends on the PAR incident on
162 the vegetation canopy during the growing season (with temperatures above 0°C), the
163 intrinsic quantum efficiency of photosynthesis (Collatz et al., 1998), and the effects of
164 photorespiration and substrate limitation at subsaturating [CO_2] represented as a function of
165 the leaf-internal [CO_2] and the photorespiratory compensation point. Leaf-internal [CO_2] is
166 estimated from ambient [CO_2] via the least-cost hypothesis (Wright et al., 2003; Prentice et
167 al., 2014) as a function of atmospheric aridity (expressed as ΔE, the climatic moisture

deficit: difference between annual (estimated) actual evapotranspiration (E_a) and equilibrium evapotranspiration (E_q)), air temperature and elevation. In the version used here, GPP is further multiplied by $\alpha^{1/4}$ (Cramer and Prentice, 1988). This correction has been found empirically to account for the reduction in the light use efficiency of GPP at very low soil moisture content, observed in flux measurements from regions with an intense dry season. The P model produces a seasonal cycle of simulated potential GPP at GWW with a peak in austral summer, similar to the seasonal cycle of GPP in the predominant (*Eucalyptus*-dominated) vegetation as calculated from measurements made at the nearby Credo flux station (C. Macfarlane, S. Prober, pers. comm. 2014; data processing by T.W. Davis, pers. comm. 2014). The fractional cover of vegetation (trees, shrubs, grasses) is about 0.1, thus the simulated potential GPP of *ca* 1.5 mol m^{-2} day^{-1} at the peak is consistent with flux-derived GPP, *ca* 0.15 mol m^{-2} day^{-1}.

Modelled potential GPP was used as input to a species-based carbon allocation and functional geometric tree-growth model (the T model: Li et al., 2014) to simulate tree growth. In the T model, the fraction of incident PAR absorbed by the canopy (fAPAR) is estimated from the leaf area index within the canopy and used to convert potential to actual GPP using Beer's law (Jarvis and Leverenz, 1983). Annual net primary production (NPP) is then derived from annual GPP, corrected for foliage respiration, by deducting growth respiration (proportional to NPP) and the maintenance respiration of sapwood and fine roots. NPP is allocated to stem, foliage and fine-root increments, foliage turnover and fine-root turnover. Carbon is allocated to different tissues within the constraint of the basic functional or geometric relationships between different dimensions of the tree, including asymptotic height-diameter trajectories (Thomas, 1996; Ishii et al., 2000; Falster and Westoby, 2005).

A full description of the coupled (PT) model is given in Li et al. (2014). The model was used to simulate the growth of *Pinus koraiensis* in a temperate, relatively moist site in the Changbai Mountains, China. Tree growth there is primarily constrained by growing-season PAR, which in turn is strongly influenced by cloud cover. When driven by local climate data and changing atmospheric [CO_2], the model produced a good representation of interannual variability in *Pinus koraiensis* growth over the past 50 years.

2.4 Derivation of model parameter values

The P model is generic for C_3 photosynthesis and has no adjustable parameters. The T model, in contrast, is species-specific and requires values for 13 parameters. Most of these could be obtained from measurements made at the sampling site, or from the literature (Table 2). Stem basal diameter, tree height and crown area were measured on 146 trees at the site. The measurements were made on all *Callitris* trees within the 500 m x 500 m plot. Parameter values for the initial slope of the height–diameter relationship (a: 41.35), the initial ratio of crown area to stem cross-sectional area (c: 626.92), and maximum tree height (H_m: 9.58 m) were estimated using non-linear regression applied to the effective basal diameter (D), tree height (H), and crown area (A_C) measurements on these 146 trees. Values for sapwood density (ρ_S) and specific leaf area (σ) were derived from five measurements made at the sampling site (Table 2). We used generic values for the extinction coefficient (k) for photosynthetically active radiation (PAR) and yield factor (y), from the literature (Table 2). Leaf area index within the crown (L) and foliage turnover time (τ_f) were estimated from published measurements on *Callitris* species in other regions of Australia.

No measurements were available for fine-root turnover time (τ_f), fine-root specific respiration rate (r_f), sapwood-specific respiration rate (r_s), and ratio of fine-root mass to foliage area (ζ) in *Callitris*, and these were not measured in the field. But their values can have a substantial impact on simulated radial growth, and on the shape of the simulated ontogenetic ageing curve (Li et al., 2014). We used approximate Bayesian parameter calibration (van der Vaart et al., 2015) to derive mutually consistent values of these four parameters The calibration target was mean ring-width during the period 1950-2012 and the posterior was constructed by sampling the joint parameter distribution 1,000,000 times and retaining the values of the 1000 samples that most closely matched the calibration target (van der Vaart et al., 2015). A constraint was imposed to ensure that there were no negative growth rates of any model component. Calibration was performed using simulations in which climate and [CO_2] varied realistically. [CO_2] data were obtained by splicing ice-core records for the interval from 1901 to 1957 (Etheridge et al., 1996; MacFarling Meure et al., 2006) with the annual average of direct atmospheric measurements from Mauna Loa and the South Pole stations from 1958 to 2013:

http://scrippsco2.ucsd.edu/data/merged_ice_core/merged_ice_core_yearly.csv.

We examined correlations among the posterior parameter values using both Pearson correlation coefficients and principal components analysis. These analyses showed no correlation among estimates of fine-root turnover time (τ_f), fine-root specific respiration rate (r_f), and sapwood-specific respiration rate (r_s). However, the ratio of fine-root mass to foliage area (ζ) was correlated with fine root turnover time (0.69) and fine root respiration rate (–0.70). The calibration produced a shift in the median value for all four parameters (Fig. 2a) and a substantial reduction in uncertainty was obtained for ζ. The final parameter

values used for all four variables lie within the range of measurements that have been made on other gymnosperms (Table 2).

2.5 Climate inputs

The P model requires inputs of daily temperature, precipitation, and fractional cloud cover, which are generally obtained by linear interpolation of monthly values of these variables (Wang et al., 2014). There are four meteorological stations (Credo, Kalgoorlie, Ora Banda, Menzies) within 100 km of the GWW site, but none has records for all three variables covering the whole interval sampled by the tree-ring series (i.e. 1920-2013). Thus, none of these local records can be used to drive the simulations. We therefore used monthly temperature, precipitation, and cloud cover fraction for the interval 1920 onwards from the CRU TS v3.22 data set (Harris et al., 2014), using values of these variables for the single grid cell (30.25°S, 120.75°E) from CRU TS v3.22 in which the sampling site lies. The CRU climate is derived using a distance-weighted interpolation from all available meteorological records and has been homogenized to remove any impacts from using information for individual climate variables from different stations or from different numbers of stations through time. Nevertheless, we examined the reliability of this approach by comparing the gridded climate values with observed values from the three meteorological stations for all overlapping intervals for each variable; in the case of solar radiation/cloud cover this was very short (post-1990 only). There is generally good agreement between the gridded monthly (and annual) temperature and precipitation data and meteorological station data with respect to long-term means, interannual variability and trends. The correlation between the gridded and observed values of interannual variability in temperature at Kalgoorlie post-1911 is 0.907 ($p < 0.001$). Similarly, the correlation between the gridded and observed

values of interannual variability in precipitation at Menzies between 1901 and 2008 is 0.905 ($p < 0.001$).

2.6 Definition of the effective growing season

The GWW is characterized by strong precipitation seasonality, while temperature variations are modest. In climates with cold winters there is always a distinct growing season, even for evergreen trees. Carbon that is assimilated after maximum leaf-out in any year is normally stored and contributes to tree growth in the subsequent growing season (Michelot et al., 2012). Thus the effective growing season for tree growth in seasonally cold climates can be defined as from mid-summer in one year until mid-summer in the subsequent year (Li et al., 2014). It is less obvious how to define the effective growing season in moisture-limited regions. However, several studies have indicated that radial growth in *Callitris* is affected not only by seasonal precipitation during the year when tree-ring growth is initiated, but also by precipitation during the wet season in previous years (Baker et al., 2008; Cullen and Grierson, 2009), suggesting that it is necessary to consider an effective growing season for carbon accumulation that is longer than the current growth year.

We investigated the optimal interval influencing carbon accumulation and tree growth using ordinary least-squares multiple linear regression. Based on likely physiological constraints in a drought-controlled environment, we used total annual photosynthetically active radiation (PAR_0), VPD, and the ratio of actual to potential evapotranspiration (α) as independent variables in the regression and mean tree-ring width during the period from 1950-2013 as the dependent variable. (PAR_0 is defined as total incident PAR during the period with temperatures > 0˚C, but for GWW this is the same as the total annual incident

289 PAR; we use the notation PAR_0 for consistency with other work using the P and T models.)
290 The post-1950 interval was used for this analysis in order to use all ten tree-ring records to
291 derive the target mean tree-ring width. We defined the effective growing season as the
292 period from January to December in the current growth year, and then extended the interval
293 by six-month steps for a period up to three years. In these latter analyses, each six-month
294 period contributes equally to the carbon available for growth. The goodness-of-fit of each
295 model was judged based on the significance of the slope coefficient of each independent
296 variable (*p* value) and the R^2 of the overall model.
297

298 The results from ordinary least-squares multiple linear regression analysis (Table 3)
299 showed that the best prediction of tree-ring width is obtained using an effective growing
300 season of two years (from January in the previous year to December in the year of the tree-
301 ring formation). This interval also produced significant *p* values for each of the predictor
302 variables (Table 3). The overall relationship, and the significance of each climate variable,
303 deteriorated when the effective growing season was defined as longer than two years.
304 Thus, in the subsequent application of the model, we used a carbon-accumulation period of
305 two years (equally-weighted mean of the two years) to drive simulated growth rates. This is
306 consistent with the observation that radial growth of *Callitris* is influenced by precipitation in
307 the previous rainy season as well as the present one (Baker et al., 2008; Cullen and
308 Grierson, 2009).
309

310 **2.7 Application of the Model**

311 Each tree was initialized with its actual effective single-stemmed basal diameter in the first
312 year of growth, except that trees that started growing before 1901 were initialized using the

actual effective single-stemmed basal diameter in 1901. The availability of climate data determined the earliest start date of the simulations (1901). The initial basal diameter was calculated from the measured diameter in August 2013 (which varied between 11.9 and 28.2 cm) and measured radial growth between the starting date and sampling date.

The model was run initially using values of the four poorly-known parameters calibrated to reproduce the mean ring-width for the period 1950-2012, with varying climate and [CO_2]. As a test of whether carbon allocation might plausibly have varied, we ran a second simulation in which the ratio of fine-root mass to foliage area (ζ) was calibrated using a spline fit to the mean ring-width during successive 30-year windows between 1920-2012, with a step of five years between windows and using appropriate [CO_2] and climate for each window.

3 Results

3.1 Baseline simulation of ring-width versus observations

The T model generally captured the amplitude of *Callitris* tree growth variations (Fig. 2b). The mean simulated ring-width for the period 1950-2012 was 0.840 mm, compared to an observed value of 0.753 mm. The standard deviation (SD) in mean ring-width (0.197 mm) was underestimated compared to the observed SD (0.215 mm). This difference probably reflects the impact of local variability in environmental conditions on individual tree growth, not accounted for in the model. Regression analysis (Fig. 3, Table 4) showed that tree growth has a strongly positive, independent response to both PAR_0 and soil moisture availability (indexed by α) and a negative response to VPD ($p < 0.01$). (Similar relationships are obtained using a linear mixed-effect model to account for autocorrelation between

337 replicates and temporally: Table 4). These relationships are captured in the simulations.
338 Although there is more scatter in the observations, the slopes of the observed and
339 simulated responses to PAR_0, α and VPD are statistically identical in the model and in the
340 data. The positive relationship with PAR_0 reflects the universal control of photosynthesis by
341 light availability, and the positive relationship with α is consistent with observations that the
342 growth of *Callitris* is strongly influenced by precipitation variability (Ash, 1983; Cullen and
343 Grierson, 2009). VPD affects stomatal conductance such that increasing VPD leads to
344 stomatal closure, with a correspondingly negative impact on photosynthesis and hence
345 carbon assimilation and growth.

346 Whereas the responses of modelled and measured ring-width to climate variables are
347 quantitatively similar, there is a discrepancy in the response to [CO_2]. The data show no
348 significant response (-0.0006 ± 0.0015 mm ppm^{-1}, $p = 0.687$) while the model shows a
349 small but significant positive response (0.0011 ± 0.0004 mm ppm^{-1}, $p = 0.004$). The
350 correlation between simulated and observed interannual variability (Fig. 2b) is not
351 significant ($r = 0.06$, $p = 0.571$), reflecting an unrealistic simulated increase during recent
352 decades. The root mean squared error (RMSE) of this simulation was 0.28 mm.

353

354 **3.2 Effects of increasing [CO_2] on tree-ring width and carbon allocation strategy**

355 Time-dependent calibration produced values of ζ that decreased by *ca* 6% from the
356 beginning of the simulation to the 30-year interval centred on 1965, and subsequently
357 increased by *ca* 12% by the 30-year interval centred on 1995 (Fig. 4). In other words, the
358 values of ζ required to match the observations increased through the period when [CO_2]
359 increased the most (*ca* 40 ppm, as compared to *ca* 12 ppm before 1965). GWW climate
360 has also varied systematically during this period. The first principal component of
361 multidecadal variability (based on 30-year means of standardized values of α, VPD and

362 PAR_0) explains 55% of the overall variance with loadings of -0.71 for both α and VPD and
363 0.00 for PAR. The second principal component explains a further 44% of the variance and
364 is related primarily to PAR (-0.87) and secondarily to α (0.36) and VPD (-0.35). The
365 changes in PAR, however, are small (ca 2%) and thus the impact of increasing moisture
366 availability during the first half of the period could explain the initial decline in ζ (Fig. 4). The
367 simulation with time-varying values of ζ produced improved correlation (r = 0.60, p < 0.001)
368 with the tree-ring observations (Fig. 5), avoiding the systematic overestimation of ring-
369 widths in recent years compared to observations that is seen in the simulation with
370 observed [CO_2] and fixed ζ (Fig. 2b). The RMSE of the modelled ring-widths was reduced
371 from 0.28 to 0.17 mm by allowing variation in ζ. The remaining discrepancies between
372 simulated and observed ring widths probably reflect simplifications in the modelling
373 approach, most particularly with respect to carbon carryover between years and the use of
374 an average value for wood density. However, the progressive nature of the changes in
375 below-ground allocation coupled with the overall improvement in the simulations both
376 indicate that it is plausible that changes in allocation play a role in the response to
377 increasing [CO_2].

378

379 ## 4 Discussion and Conclusions

380 The dependencies of *Callitris columellaris* radial growth on climate at GWW could be
381 simulated by coupling a generic model of GPP (P) with a model of carbon allocation and
382 functional geometric tree growth (T), using species-specific parameter values in T. Model
383 performance was not adversely affected by the reduction in winter precipitation, and the
384 shift to less frequent but more intense precipitation events, that occurred in latter part of the

record. Radial growth was positively related to PAR_0 and α, and negatively correlated with VPD, with similar quantitative dependencies shown in the data and in the model.

The response to VPD can be explained as a consequence of the atmospheric control on stomatal conductance and hence photosynthesis. Thus, both atmospheric and soil moisture deficits (the former indexed by VPD, the latter by α) separately influence radial growth. Previous studies have shown that the growth of *Callitris* in southwestern Australia is controlled by precipitation (Sgherza et al., 2010), but there is only a weak correlation between stable carbon isotope measurements and precipitation of the current year because *Callitris* has a strong water-conservation strategy. These findings are consistent with the observed response to VPD and further support our use of a two-year period contributing to carbon accumulation and growth.

The radial growth of *Callitris columellaris* in the GWW has not responded to the [CO_2] increase of recent decades. The lack of a response to [CO_2] has been a feature of other quantitative studies of tree growth (e.g. Kienast and Luxmoore, 1988; Archer et al., 1995; Gedalof and Berg, 2010; Peñuelas et al., 2011). Analyses of stable carbon isotopes and growth of tropical trees (van der Sleen et al., 2015) showed an increase in water-use efficiency, yet no stimulation of radial growth due to CO_2 fertilization over the past 150 years. The modelled response of ring-width to [CO_2] in our analysis was small compared with the responses to α, VPD and PAR_0 – as can be seen by comparing standardized regression coefficients for the modelled ring-widths, which are three to six times smaller for [CO_2] than for the climate variables (Table 4). A modest shift in carbon allocation (towards

408 the production of fine roots, as implied by increasing ζ) would be sufficient to reconcile the
409 modelled increase in GPP with the lack of any observed increase in ring-width.

410

411 Although the data presented here do not allow us to statistically disentangle potential
412 effects of climate variability and [CO_2] on carbon allocation patterns, we note that an
413 increase in fine-root production has been observed at the majority of Free Air Carbon
414 dioxide Enrichment (FACE) sites. Therefore, it is reasonable to speculate that an increase
415 in ζ might come about as a consequence of increased [CO_2]. FACE experiments are
416 equivocal about the impact of enhanced [CO_2] on tree growth, but the shift in allocation is a
417 common feature. The Swiss Canopy Crane site is an outlier, with decreased below-ground
418 allocation (Bader et al., 2009). We might expect *a priori* that trees at sites experiencing
419 strong nutrient limitation would show this kind of response because of the need to extract
420 more nutrients to support increased NPP, whereas trees at sites experiencing strong water
421 limitation might show the opposite response due to enhanced water use efficiency at high
422 [CO_2]. Our results do not support this reasoning, however, suggesting instead that the trees
423 may be allocating more below ground as [CO_2] increases even in the strongly water-limited
424 environment of the GWW. Increased below-ground allocation could in part represent carbon
425 export to mycorrhizae or the rhizosphere (Godbold et al., 2015), which is not considered in
426 the T model.

427

428 Appropriately analysed, tree-ring records worldwide should yield consistent information
429 about the diverse responses of tree growth and allocation to environmental change. Here,
430 with the use of a simple process-based model of tree growth, we have explored the
431 potential for changes in the proportion of above- and below-ground allocation to explain the

lack of evidence for increased radial growth in response to recent increases in [CO_2]. A noteworthy feature of our study is that a relatively minor change in the relative allocation of carbon to fine roots *versus* leaves is sufficient to suppress an increase in radial growth in response to increasing [CO_2] in the simulations. If such changes in allocation occur in the real world, then the observed stability in radial growth in recent decades does not mean that GPP or NPP is unresponsive to [CO_2] (whether through nutrient limitation, sink limitation or any other mechanism). There are a number of potential sources of uncertainty in our modelling approach, including the representation of aging trends and of the importance of the carry-over of non-structural carbohydrates between growing seasons. Nevertheless, our results support the idea that above-ground biomass production and radial growth are sensitive to environmental effects on carbon allocation. This is important because the influence of environmental conditions on allocation are neglected by most current ecosystem models (De Kauwe et al., 2014).

Acknowledgements

We thank Henrique Togashi for assistance in making the SLA and sapwood density measurements in GWW. GL was supported by International Postgraduate Research Scholarship at Macquarie University. The work is a contribution to the AXA Chair programme on Biosphere and Climate Impacts and the Imperial College initiative Grand Challenges in Ecosystems and the Environment. The GWW SuperSite is a node in the Terrestrial Ecosystem Research Network (TERN), supported by the Australian SuperSites facility of TERN.

References

Ainsworth, E.A., Long, S.P., 2005. What have we learned from 15 years of free-air CO_2 enrichment (FACE)? A meta-analytic review of the responses of photosynthesis, canopy properties and plant production to rising CO_2. New Phytol. 165, 351-372.

Ansell, T., Reason, C., Smith, I., Keay, K., 2000. Evidence for decadal variability in southern Australian rainfall and relationships with regional pressure and sea surface temperature. Int. J. Climatol. 20, 1113-1129.

Archer, S., Schimel, D.S., Holland, E.A., 1995. Mechanisms of shrubland expansion: land use, climate or CO_2? Clim. Chang. 29, 91-99.

Ash, J., 1983. Tree rings in tropical Callitris macleayana F. Muell. Aust. J. Bot. 31, 277-281.

Bader, M., Hiltbrunner, E., Körner, C., 2009. Fine root responses of mature deciduous forest trees to free air carbon dioxide enrichment (FACE). Funct. Ecol. 23, 913-921.

Baker, P.J., Palmer, J.G., D'Arrigo, R., 2008. The dendrochronology of Callitris intratropica in northern Australia: annual ring structure, chronology development and climate correlations. Aust. J. Bot. 56, 311-320.

Battipaglia, G., Saurer, M., Cherubini, P., Calfapietra, C., McCarthy, H.R., Norby, R.J., Francesca Cotrufo, M., 2013. Elevated CO_2 increases tree-level intrinsic water use efficiency: insights from carbon and oxygen isotope analyses in tree rings across three forest FACE sites. New Phytol. 197, 544-554.

Boucher, É., Guiot, J., Hatté, C., Daux, V., Danis, P.A., Dussouillez, P., 2014. An inverse modeling approach for tree-ring-based climate reconstructions under changing atmospheric CO_2 concentrations. Biogeosciences 11, 3245-3258.

Burrows, W., Hoffman, M., Compton, J., Back, P., 2001. Allometric relationship and community stocks in white cypress pine (Callitris glaucophylla) and associated eucalypts in the Carnarvon area-south central Queensland. Australian Greenhouse Office, Canberra.

Burton, A.J., Pregitzer, K.S., 2002. Measurement carbon dioxide concentration does not affect root respiration of nine tree species in the field. Tree Physiol. 22, 67-72.

Cai, W., Cowan, T., 2006. SAM and regional rainfall in IPCC AR4 models: Can anthropogenic forcing account for southwest Western Australian winter rainfall reduction? Geophys. Res. Lett. 33.

Calfapietra, C., Gielen, B., Galema, A., Lukac, M., De Angelis, P., Moscatelli, M., Ceulemans, R., Scarascia-Mugnozza, G., 2003. Free-air CO_2 enrichment (FACE) enhances biomass production in a short-rotation poplar plantation. Tree Physiol. 23, 805-814.

Collatz, G.J., Berry, J.A., Clark, J.S., 1998. Effects of climate and atmospheric CO_2 partial pressure on the global distribution of C4 grasses: present, past, and future. Oecologia 114, 441-454.

Cramer, W., Prentice, I.C., 1988. Simulation of regional soil moisture deficits on a European scale. Nor. Geogr. Tidsskr. Nor. J. Geogr. 42, 149-151.

Cullen, L.E., Adams, M.A., Anderson, M.J., Grierson, P.F., 2008. Analyses of $\delta^{13}C$ and δ18O in tree rings of Callitris columellaris provide evidence of a change in stomatal control of photosynthesis in response to regional changes in climate. Tree Physiol. 28, 1525-1533.

500 Cullen, L.E., Grierson, P.F., 2007. A stable oxygen, but not carbon, isotope chronology of
501 Callitris columellaris reflects recent climate change in north-western Australia. Clim.
502 Change 85, 213-229.

503 Cullen, L.E., Grierson, P.F., 2009. Multi-decadal scale variability in autumn-winter rainfall in
504 south-western Australia since 1655 AD as reconstructed from tree rings of Callitris
505 columellaris. Clim. Dynam. 33, 433-444.

506 De Kauwe, M.G., Medlyn, B.E., Zaehle, S., Walker, A.P., Dietze, M.C., Hickler, T., Jain,
507 A.K., Luo, Y., Parton, W.J., Prentice, I.C., 2013. Forest water use and water use
508 efficiency at elevated CO_2: a model-data intercomparison at two contrasting
509 temperate forest FACE sites. Glob. Chang. Biol. 19, 1759-1779.

510 De Kauwe, M.G., Medlyn, B.E., Zaehle, S., Walker, A.P., Dietze, M.C., Wang, Y.P., Luo, Y.,
511 Jain, A.K., El-Masri, B., Hickler, T., 2014. Where does the carbon go? A model and
512 data intercomparison of vegetation carbon allocation and turnover processes at two
513 temperate forest free-air CO_2 enrichment sites. New Phytol. 203, 883-899.

514 DeLucia, E.H., Hamilton, J.G., Naidu, S.L., Thomas, R.B., Andrews, J.A., Finzi, A., Lavine,
515 M., Matamala, R., Mohan, J.E., Hendrey, G.R., 1999. Net primary production of a
516 forest ecosystem with experimental CO_2 enrichment. Science 284, 1177-1179.

517 Drake, B.G., Gonzàlez-Meler, M.A., Long, S.P., 1997. More efficient plants: a consequence
518 of rising atmospheric CO_2? Annu. Rev. Plant. Biol. 48, 609-639.

519 Etheridge, D., Steele, L., Langenfelds, R., Francey, R., Barnola, J.M., Morgan, V., 1996.
520 Natural and anthropogenic changes in atmospheric CO_2 over the last 1000 years
521 from air in Antarctic ice and firn. J. Geophys. Res. 101, 4115-4128.

522 Falster, D.S., Westoby, M., 2005. Tradeoffs between height growth rate, stem persistence
523 and maximum height among plant species in a post-fire succession. Oikos 111, 57-
524 66.

525 Fieber, K.D., Davenport, I.J., Tanase, M.A., Ferryman, J.M., Gurney, R.J., Walker, J.P.,
526 Hacker, J.M., 2014. Effective LAI and CHP of a single tree from small-footprint full-
527 vaveform LiDAR. IEEE Geosci. Remote Sens. Lett. 11, 1634-1638.

528 Field, C., Merino, J., Mooney, H.A., 1983. Compromises between water-use efficiency and
529 nitrogen-use efficiency in five species of California evergreens. Oecologia 60, 384-
530 389.

531 Gedalof, Z., Berg, A.A., 2010. Tree ring evidence for limited direct CO_2 fertilization of
532 forests over the 20th century. Glob. Biogeochem. Cycles 24, GB3027,
533 doi:10.1029/2009GB003699.

534 Girardin, M.P., Bernier, P.Y., Raulier, F., Tardif, J.C., Conciatori, F., Guo, X.J., 2011.
535 Testing for a CO2 fertilization effect on growth of Canadian boreal forests. Journal of
536 Geophysical Research 116, G01012.

537 Godbold, D.L., Vašutová, M., Wilkinson, A., Edwards-Jonášová, M., Bambrick, M., Smith,
538 A.R., Pavelka, M., Cudlin, P., 2015. Elevated atmospheric CO_2 affects
539 ectomycorrhizal species abundance and increases sporocarp production under field
540 conditions. Forests 6, 1256-1273.

541 Harris, I., Jones, P.D., Osborn, T.J., Lister, D.H., 2014. Updated high-resolution grids of
542 monthly climatic observations–the CRU TS3.10 Dataset. Int. J. Climatol. 34, 623-
543 642.

544 Holmes, R.L., 1983. Computer-assisted quality control in tree-ring dating and
545 measurement. Tree-ring Bull. 43, 69-78.

546 Hope, P.K., Drosdowsky, W., Nicholls, N., 2006. Shifts in the synoptic systems influencing
547 southwest Western Australia. Clim. Dynam. 26, 751-764.

548 Hyvönen, R., Ågren, G.I., Linder, S., Persson, T., Cotrufo, M.F., Ekblad, A., Freeman, M.,
549 Grelle, A., Janssens, I.A., Jarvis, P.G., 2007. The likely impact of elevated [CO_2],
550 nitrogen deposition, increased temperature and management on carbon
551 sequestration in temperate and boreal forest ecosystems: a literature review. New
552 Phytol. 173, 463-480.

553 Ishii, H., Reynolds, J.H., Ford, E.D., Shaw, D.C., 2000. Height growth and vertical
554 development of an old-growth *Pseudotsuga-Tsuga* forest in southwestern
555 Washington State, USA. Can. J. Forest Res. 30, 17-24.

556 Jarvis, P., Leverenz, J., 1983. Productivity of temperate, deciduous and evergreen forests,
557 Physiological Plant Ecology IV. Springer, Berlin Heidelberg, pp. 233-280.

558 Kienast, F., Luxmoore, R.J., 1988. Tree-ring analysis and conifer growth responses to
559 increased atmospheric CO_2 levels. Oecologia 76, 487-495.

560 King, J., Pregitzer, K., Zak, D., Sober, J., Isebrands, J., Dickson, R., Hendrey, G.,
561 Karnosky, D., 2001. Fine-root biomass and fluxes of soil carbon in young stands of
562 paper birch and trembling aspen as affected by elevated atmospheric CO_2 and
563 tropospheric O_3. Oecologia 128, 237-250.

564 Landsberg, J.J., Sands, P., 2010. Physiological Ecology of Forest Production: Principles,
565 Processes and Models. Academic Press.

566 Lee, P.S., Mackey, B.G., Berry, S.L., 2013. Modelling vegetation structure-based bird
567 habitat resources in Australian temperate woodlands, using multi-sensors. Eur. J.
568 Remote Sens. 46, 641-674.

569 Li, G., Harrison, S.P., Prentice, I.C., Falster, D., 2014. Simulation of tree-ring widths with a
570 model for primary production, carbon allocation, and growth. Biogeosciences 11,
571 6711-6724.

572 Lukac, M., Calfapietra, C., Godbold, D.L., 2003. Production, turnover and mycorrhizal
573 colonization of root systems of three *Populus* species grown under elevated CO_2
574 (POPFACE). Glob. Chang. Biol. 9, 838-848.

575 MacFarling Meure, C., Etheridge, D., Trudinger, C., Steele, P., Langenfelds, R., Van
576 Ommen, T., Smith, A., Elkins, J., 2006. Law Dome CO_2, CH_4 and N_2O ice core
577 records extended to 2000 years BP. Geophys. Res. Lett. 33.

578 Michelot, A., Simard, S., Rathgeber, C., Dufrêne, E., Damesin, C., 2012. Comparing the
579 intra-annual wood formation of three European species (*Fagus sylvatica*, *Quercus*
580 *petraea* and *Pinus sylvestris*) as related to leaf phenology and non-structural
581 carbohydrate dynamics. Tree Physiol. 32, 1033–1045.

582 Norby, R.J., Ledford, J., Reilly, C.D., Miller, N.E., O'Neill, E.G., 2004. Fine-root production
583 dominates response of a deciduous forest to atmospheric CO_2 enrichment. Proc.
584 Natl. Acad. Sci. U.S.A 101, 9689-9693.

585 Norby, R.J., Zak, D.R., 2011. Ecological lessons from free-air CO_2 enrichment (FACE)
586 experiments. Annu. Rev. Ecol. Evol. Syst. 42, 181.

587 Peñuelas, J., Canadell, J.G., Ogaya, R., 2011. Increased water-use efficiency during the
588 20th century did not translate into enhanced tree growth. Glob. Ecol. Biogeogr. 20,
589 597–608.

590 Pierce, L.L., Running, S.W., 1988. Rapid estimation of coniferous forest leaf area index
591 using a portable integrating radiometer. Ecology, 1762-1767.

592 Prentice, I.C., Dong, N., Gleason, S.M., Maire, V., Wright, I.J., 2014. Balancing the costs of
593 carbon gain and water transport: testing a new theoretical framework for plant
594 functional ecology. Ecol. Lett. 17, 82-91.

595 Pritchard, S.G., Strand, A.E., McCormack, M., Davis, M.A., Finzi, A.C., Jackson, R.B.,
596 Matamala, R., Rogers, H.H., Oren, R., 2008. Fine root dynamics in a loblolly pine
597 forest are influenced by free-air-CO_2-enrichment: A six-year-minirhizotron study.
598 Glob. Change Biol. 14, 588-602.

599 Prober, S.M., Thiele, K.R., Rundel, P.W., Yates, C.J., Berry, S.L., Byrne, M., Christidis, L.,
600 Gosper, C.R., Grierson, P.F., Lemson, K., 2012. Facilitating adaptation of
601 biodiversity to climate change: a conceptual framework applied to the world's largest
602 Mediterranean-climate woodland. Clim. Chang. 110, 227-248.

603 Schulman, E., 1956. Dendroclimatic changes in semiarid America. University of Arizona
604 Press, Tucson.

605 Sgherza, C., Cullen, L.E., Grierson, P.F., 2010. Climate relationships with tree-ring width
606 and $\delta^{13}C$ of three *Callitris* species from semiarid woodlands in south-western
607 Australia. Aust. J. Bot. 58, 175-187.

608 Smith, A.R., Lukac, M., Bambrick, M., Miglietta, F., Godbold, D.L., 2013. Tree species
609 diversity interacts with elevated CO_2 to induce a greater root system response. Glob.
610 Change Biol. 19, 217-228.

611 Smith, R.L., Tebaldi, C., Nychka, D., Mearns, L.O., 2009. Bayesian modeling of uncertainty
612 in ensembles of climate models. J. Am. Stat. Assoc. 104, 97-116.

613 Sturman, A.P., Tapper, N.J., 1996. The Weather and Climate of Australia and New
614 Zealand. Oxford University Press, Melbourne, Oxford, Auckland, and New York.

615 Thomas, S.C., 1996. Asymptotic height as a predictor of growth and allometric
616 characteristics in Malaysian rain forest trees. Am. J. Bot., 556-566.

617 van der Sleen, P., Groenendijk, P., Vlam, M., Anten, N.P., Boom, A., Bongers, F., Pons,
618 T.L., Terburg, G., Zuidema, P.A., 2015. No growth stimulation of tropical trees by 150
619 years of CO_2 fertilization but water-use efficiency increased. Nat. Geosci. 8, 24-28.

620 van der Vaart, E., Beaumont, M. A., Johnston, A. S., Sibly, R. M., 2015. Calibration and
621 evaluation of individual-based models using Approximate Bayesian Computation.
622 Ecol. Model., 312, 182-190.

623 van Ommen, T.D., Morgan, V., 2010. Snowfall increase in coastal East Antarctica linked
624 with southwest Western Australian drought. Nat. Geosci. 3, 267-272.

625 Wang, H., Prentice, I.C., Davis, T., 2014. Biophysical constraints on gross primary
626 production by the terrestrial biosphere. Biogeosciences 11, 5987-6001.

627 Watson, A., 2008. The Extraordinary Nature of the Great Western Woodlands. Wilderness
628 Society of Western Australia.

629 White, M.A., Thornton, P.E., Running, S.W., Nemani, R.R., 2000. Parameterization and
630 sensitivity analysis of the BIOME-BGC terrestrial ecosystem model: net primary
631 production controls. Earth Interact. 4, 1-85.

632 Wright, I.J., Reich, P.B., Westoby, M., 2003. Least-cost input mixtures of water and nitrogen
633 for photosynthesis. Amer. Nat. 161, 98-111.

634 Wright, I.J., Westoby, M., 2002. Leaves at low versus high rainfall: coordination of structure,
635 lifespan and physiology. New Phytol. 155, 403-416.

636 Yuan, Z., Chen, H.Y., 2010. Fine root biomass, production, turnover rates, and nutrient
637 contents in boreal forest ecosystems in relation to species, climate, fertility, and
638 stand age: literature review and meta-analyses. Crit. Rev. Plant Sci. 29, 204-221.

639 Zhang, Y., Xu, M., Chen, H., Adams, J., 2009. Global pattern of NPP to GPP ratio derived
640 from MODIS data: effects of ecosystem type, geographical location and climate.
641 Glob. Ecol. Biogeogr. Lett. 18, 280-290.

642

643

644 **Table and Figure Captions**

645

646 Table 1. Standard summary statistics for the tree-ring series. Values are given both for the
647 period 1920-2012 and for the period post-1950, because there are only a limited number of
648 individual trees represented in the first 30 year period.

649 Table 2. Definition of T model parameters and derivation of parameter values. Most of the
650 values were obtained from field measurements, or are generic. For those values estimated
651 using Bayesian calibration, we show the range of values given for *Callitris* (or related
652 species) in the literature, the prior values used in the calibration, the posterior values and
653 uncertainties, and the value used in the final model. The units are defined in the parameter
654 column, except in the case of sapwood specific respiration where the measurements are in
655 a different unit from the model parameter (and therefore specified explicitly). Values for
656 most parameters fall in well-behaved ranges, but there are large differences in the available
657 measurements of sapwood specific respiration rate and for ratio of fine-root mass to foliage
658 area and we therefore give the individual measurements rather than a range for these
659 parameters.

660

661 Table 3. Regression analysis of relationship between ring-width and climate parameters
662 using different definitions of the effective growing season, based on the interval from 1950
663 to present. The dependent variable is mean ring-width. The independent variables are the
664 total incident photosynthetically active radiation (PAR_0), vapour pressure deficit (VPD), and
665 the ratio of actual to potential evapotranspiration (α). This analysis indicates that the
666 optimum period contributing to tree growth is two years.

667

668 Table 4. Regression analyses of simulated and observed response of tree growth to climate
669 variables and CO_2. The dependent variable is mean radial growth series of the ten trees
670 (from 1950 to 2012). The independent variables are the total incident photosynthetically
671 active radiation (PAR_0), the ratio of actual to potential evapotranspiration (α), vapour
672 pressure deficit (VPD) and monthly [CO_2]. Above: analysis based on untransformed
673 variables. Middle: analysis based on standardized variables. Below: linear mixed model
674 analysis based on standardized variables.

675

676 Figure 1. Interannual variability in tree-ring widths of *Callitris columellaris* from the Great
677 Western Woodlands, Western Australia. In the top panel, the black line is the mean of the
678 observations, and the grey bars show the standard deviation (SD) of the individual sampled
679 trees. The blue line in the bottom panel shows the number of trees sampled for each
680 interval.

681

682 Figure 2. a) Prior (dashed line) and posterior (solid line) probability distribution functions for
683 fine-root turnover time (τ_r), fine-root specific respiration rate (r_r), sapwood-specific
684 respiration rate (r_s); ratio of fine-root mass to foliage area (ζ). b) Comparison between
685 simulated and observed tree-ring widths, for the period 1920 to the present, using varying
686 climate and [CO_2]. The black line is the mean of the observations, and the grey bars are the
687 standard deviation (SD) among the ten individual trees sampled. The blue line and bars are
688 the mean and standard deviation for the ten simulated individual trees.

689

690 Figure 3. Simulated and observed response of tree radial growth to major climate variables
691 and [CO_2]: partial residual plots based on the regression analysis, obtained using the *visreg*

692 package in R, are shown. The dependent variable is mean ring-width (from 1950 to 2012).
693 The predictor variables are total incident photosynthetically active radiation (PAR_0), vapour
694 pressure deficit (VPD), the ratio of actual to potential evapotranspiration (α), and monthly
695 [CO_2].
696
697 Figure 4. Time-dependent variation of the ratio of fine-root mass to foliage area (ζ)
698 estimated by approximate Bayesian calibration. The graph shows the percentage change to
699 the mean value of ζ for 30-year moving windows since 1920 (red), using the appropriate
700 [CO_2] and α for each window. Values on the *x*-axis are plotted against the middle year of
701 each 30-year window. Also shown are [CO_2] (grey) and the first principal component of the
702 multidecadal variability in climate (α, VPD, PAR_0) (blue).
703
704 Figure 5. Simulation of radial growth in response to changing climate and observed [CO_2],
705 allowing for the effect of changing allocation to fine roots. The black line is the mean of the
706 observations, and the grey bars are the standard deviation (SD) among the ten individual
707 trees sampled. The blue line and bars are the mean and standard deviation for the ten
708 simulated individual trees.
709

710 Table 1. Standard summary statistics for the tree-ring series. Values are given both for the
711 period 1920-2012 and for the period post-1950, because there are only a limited number of
712 individual trees represented in the first 30-year period.
713

Interval	1920-2012	1950-2012
Mean	0.482	0.4825
Standard deviation	0.321875	0.324125
First order autocorrelation	0.20521875	0.19253125
Mean correlation among all radii	0.137	0.147
Mean correlation between trees	0.128	0.136
Mean correlation within trees	0.237	0.259
Signal-to-noise ratio	2.912	3.3
Expressed population signal	0.744	0.767

714

715 Table 2. Definition of T model parameters and derivation of parameter values. Most of the values were obtained from field measurements,
716 or are generic. For those values estimated using Bayesian calibration, we show the range of values given for *Callitris* (or related species)
717 in the literature, the prior values used in the calibration, the posterior values and uncertainties, and the value used in the final model. The
718 units are defined in the parameter column, except in the case of sapwood specific respiration where the measurements are in a different
719 unit from the model parameter (and therefore specified explicitly). Values for most parameters fall in well-behaved ranges, but there are
720 large differences in the available measurements of sapwood specific respiration rate and for ratio of fine-root mass to foliage area and we
721 therefore give the individual measurements rather than a range for these parameters.

Parameter	*Symbol*	Uncertainty or range of values from literature	Source of information	Prior value	Posterior value	Accepted value	Reference
initial slope of height-diameter relationship (–)	a	41.35 ± 2.58	observation	-	-	41.35	-
initial ratio of crown area to stem cross-sectional area (–)	c	626.92 ± 20.03	observation	-	-	626.92	-
maximum tree height (m)	H_m	9.58 ± 1.11	observation	-	-	9.58	-
sapwood density (kg C m-3)	ρ_s	406 ± 32	observation	-	-	406	-
specific leaf area (m2 kg-1 C)	σ	5.16 ± 0.32	observation	-	-	5.16	-
leaf area index within the crown (–)	L	1.87 ± 0.18	species-specific literature value	-	-	1.87	Fieber et al., 2014
foliage turnover time (yr)	τ_f	2.58	species-specific literature value	-	-	2.58	Wright and Westoby, 2002
PAR extinction coefficient (–)	k	0.48-0.58	generic value	-	-	0.5	Pierce and Running, 1988
yield factor (–)	Y	0.5-0.7	generic value	-	-	0.6	Zhang et al., 2009
fine-root turnover time (yr)	τ_r	0.76 ± 0.06	Bayesian parameter optimization	0.75 ± 0.5	1.00 ± 0.40	1.00	Yuan and Chen, 2010 (estimation for evergreen needleleaf trees)
fine-root specific respiration rate (yr-1)	r_r	1.36	Bayesian parameter optimization	1.36± 1	1.23 ± 0.74	1.23	Burton and Prigitzer, 2002 (estimation from one-seeded Juniper)
sapwood specific respiration rate (yr-1)	r_s	0.5-10, 20 nmol mol–1 s–1	Bayesian parameter optimization	1 ± 0.75 nmol mol–1 s–1	1.16 ± 0.66 nmol mol–1 s–1	1.16 nmol mol–1 s–1 (0.034 yr-1)	Landsberg and Sands, 2010
ratio of fine-root mass to foliage area (kgC m-2)	ζ	1.0; 0.17	Bayesian parameter optimization	0.6 ± 0.5	0.150 ± 0.052	0.150	Burrows et al., 2001 (estimation for Callitris); White et al. (2000) (estimation for evergreen needleleaf tree)

722

Table 3. Regression analysis of relationship between ring-width and climate parameters using different definitions of the effective growing season, based on the interval from 1950 to present. The dependent variable is mean ring-width. The independent variables are the total incident photosynthetically active radiation (PAR_0), vapour pressure deficit (VPD), and the ratio of actual to potential evapotranspiration (α). This analysis indicates that the optimum period contributing to tree growth is two years.

		PAR_0 (mm (kmol photon $m^{-2})^{-1}$)	VPD (mm hPa^{-1})	α (mm)	R^2
Formation year	Estimation	0.48	–0.11	0.8	
	Standard error	± 0.20	± 0.04	±0.4	0.184
	p value	0.020	0.016	0.069	
Calendar year	Estimation	0.43	–0.06	0.6	
	Standard error	± 0.20	± 0.04	± 0.6	0.094
	p value	0.039	0.171	0.266	
1.5 Calendar years	Estimation	0.68	–0.14	1.4	
	Standard error	± 0.22	± 0.05	± 0.5	0.286
	p value	0.004	0.007	0.009	
2 Calendar years	Estimation	0.70	–0.17	1.7	
	Standard error	± 0.24	± 0.05	± 0.5	0.345
	p value	0.006	0.002	0.003	
2.5 Calendar years	Estimation	0.67	–0.16	1.7	
	Standard error	± 0.27	± 0.06	± 0.6	0.269
	p value	0.017	0.010	0.009	
3 Calendar years	Estimation	0.94	–0.20	2.0	
	Standard error	± 0.29	± 0.07	± 0.7	0.293
	p value	0.002	0.004	0.004	

Table 4. Regression analyses of simulated and observed response of tree growth to climate variables and CO_2. The dependent variable is mean radial growth series of the ten trees (from 1950 to 2012). The independent variables are the total incident photosynthetically active radiation (PAR_0), the ratio of actual to potential evapotranspiration (α), vapour pressure deficit (VPD) and monthly [CO_2]. Above: analysis based on untransformed variables. Middle: analysis based on standardized variables. Below: linear mixed model analysis based on standardized variables.

Untransformed linear model		PAR_0 (mm (kmol photon $m^{-2})^{-1}$)	α (mm)	VPD (mm hPa^{-1})	CO_2 (mm ppm^{-1})
Observation	Estimation	0.709	1.734	−0.164	−0.001
	Standard error	±0.246	±0.572	±0.059	±0.001
	p value	0.006	0.004	0.008	0.687
Simulation with actual CO_2	Estimation	0.762	2.308	−0.096	0.001
	Standard error	±0.059	±0.137	±0.014	±0.000
	p value	<0.001	<0.001	<0.001	0.004
Simulation with time-dependent ζ and actual CO_2	Estimation	0.622	2.221	−0.060	-0.001
	Standard error	±0.102	±0.224	±0.023	±0.001
	p value	<0.001	<0.001	0.014	0.113

Standardized linear model		PAR_0	α	VPD	CO_2
Observation	Estimation	0.095	0.085	−0.099	−0.011
	Standard error	±0.033	±0.028	±0.036	±0.027
	p value	0.006	0.004	0.008	0.687
Simulation with actual CO_2	Estimation	0.102	0.113	−0.058	0.020
	Standard error	±0.008	±0.007	±0.008	±0.007
	p value	<0.001	<0.001	<0.001	0.004
Simulation with time-dependent ζ and actual CO_2	Estimation	0.088	0.110	−0.034	-0.017
	Standard error	±0.014	±0.011	±0.013	±0.011
	p value	<0.001	<0.001	0.014	0.113

Standardized linear mixed model		PAR_0	α	VPD	CO_2
Observation	Estimation	0.096	0.089	−0.095	−0.013
	Standard error	±0.034	±0.039	±0.039	±0.057
	p value	0.005	0.010	0.029	0.825
Simulation with actual CO_2	Estimation	0.090	0.110	−0.057	0.029
	Standard error	±0.006	±0.006	±0.008	±0.008
	p value	<0.001	<0.001	<0.001	0.019
Simulation with time-dependent ζ and actual CO_2	Estimation	0.085	0.103	−0.050	-0.001
	Standard error	±0.009	±0.005	±0.007	±0.001
	p value	<0.001	<0.001	<0.001	1

742

743

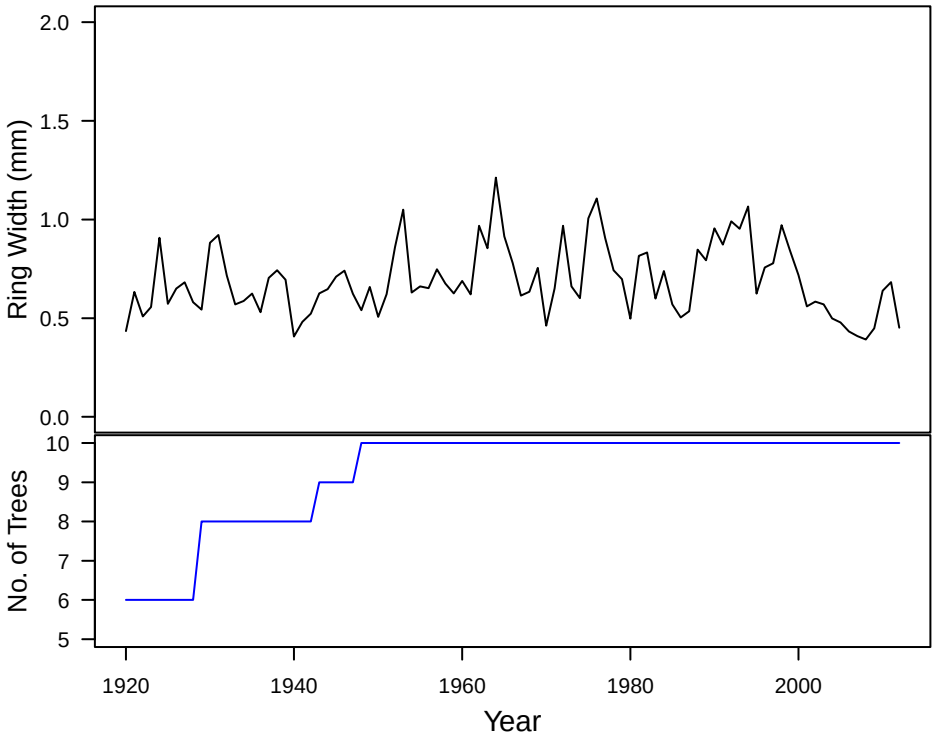

744

745 Figure 1. Interannual variability in tree-ring widths of *Callitris columellaris* from the Great
746 Western Woodlands, Western Australia. In the top panel, the black line is the mean of the
747 observations, and the grey bars show the standard deviation (SD) of the individual
748 sampled trees. The blue line in the bottom panel shows the number of trees sampled for
749 each interval.

750

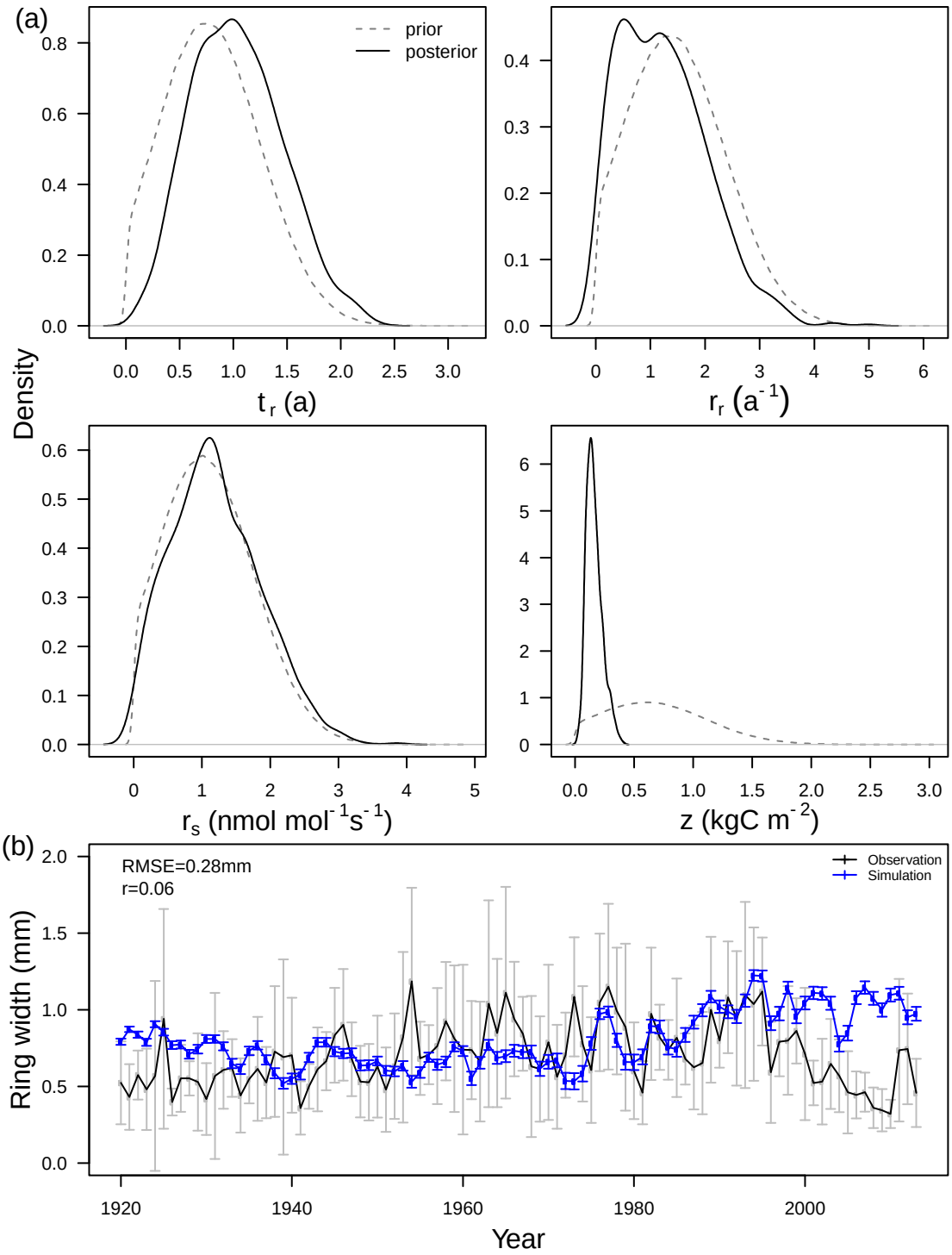

751

752 Figure 2. a) Prior (dashed line) and posterior (solid line) probability distribution function for
753 fine-root turnover time (τ_f), fine-root specific respiration rate (r_f), sapwood-specific
754 respiration rate (r_S); ratio of fine-root mass to foliage area (ζ). b) Comparison between
755 simulated and observed tree-ring widths, for the period 1920 to the present, using varying
756 climate and [CO_2]. The black line is the mean of the observations, and the grey bars are

757 the standard deviation (SD) among the ten individual trees sampled. The blue line and
758 bars are the mean and standard deviation for the ten simulated individual trees.

759

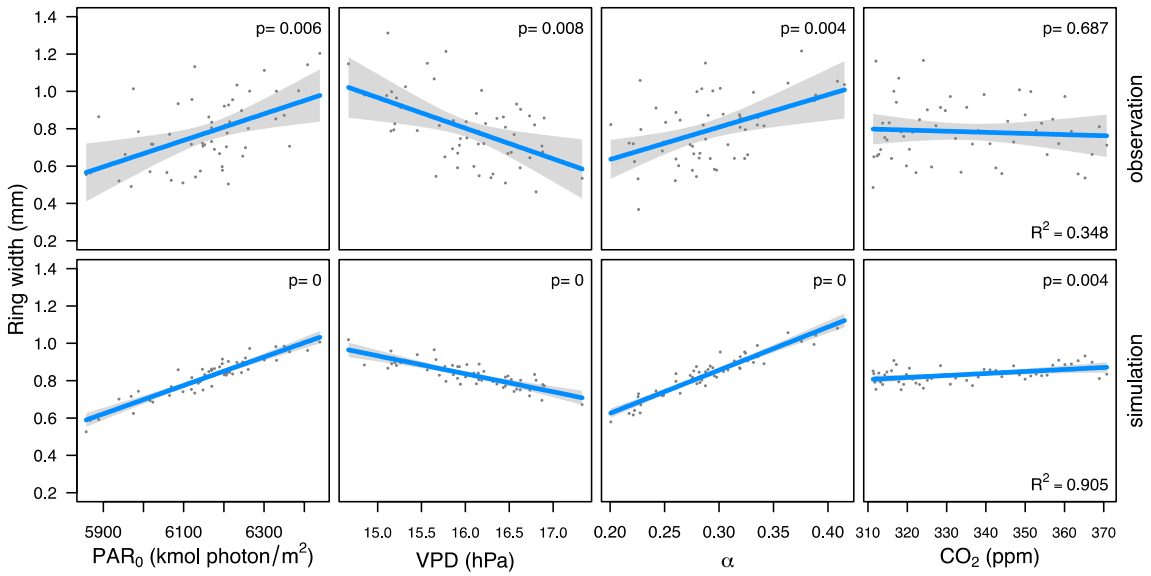

760

761 Figure 3. Simulated and observed responses of tree radial growth to climate variables and
762 [CO_2]: partial residual plots based on the regression analysis, obtained using the *visreg*
763 package in R, are shown. The dependent variable is mean ring-width (from 1950 to 2012).
764 The predictor variables are annual incident photosynthetically active radiation (PAR_0),
765 vapour pressure deficit (VPD), the ratio of actual to potential evapotranspiration (α), and
766 monthly [CO_2].

767
768

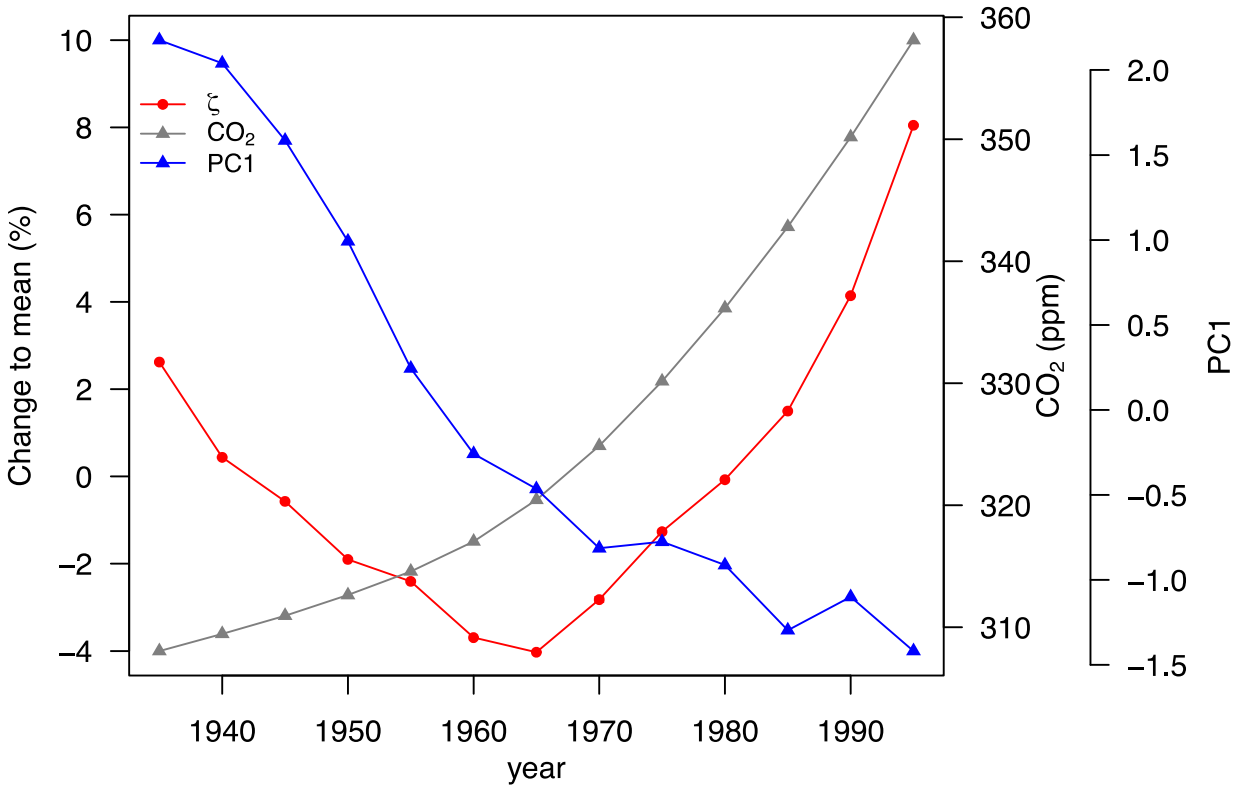

769

770 Figure 4. Time-dependent variation of the ratio of fine-root mass to foliage area (ζ)
771 estimated by approximate Bayesian calibration. The graph shows the percentage change
772 to the mean value of ζ for 30-year moving windows since 1920 (red), using the appropriate
773 [CO_2] and α for each window. Values on the *x*-axis are plotted against the middle year of
774 each 30-year window. Also shown are [CO_2] (grey) and the first principal component of the
775 multidecadal variability in climate (α, VPD, PAR_0) (blue).

776

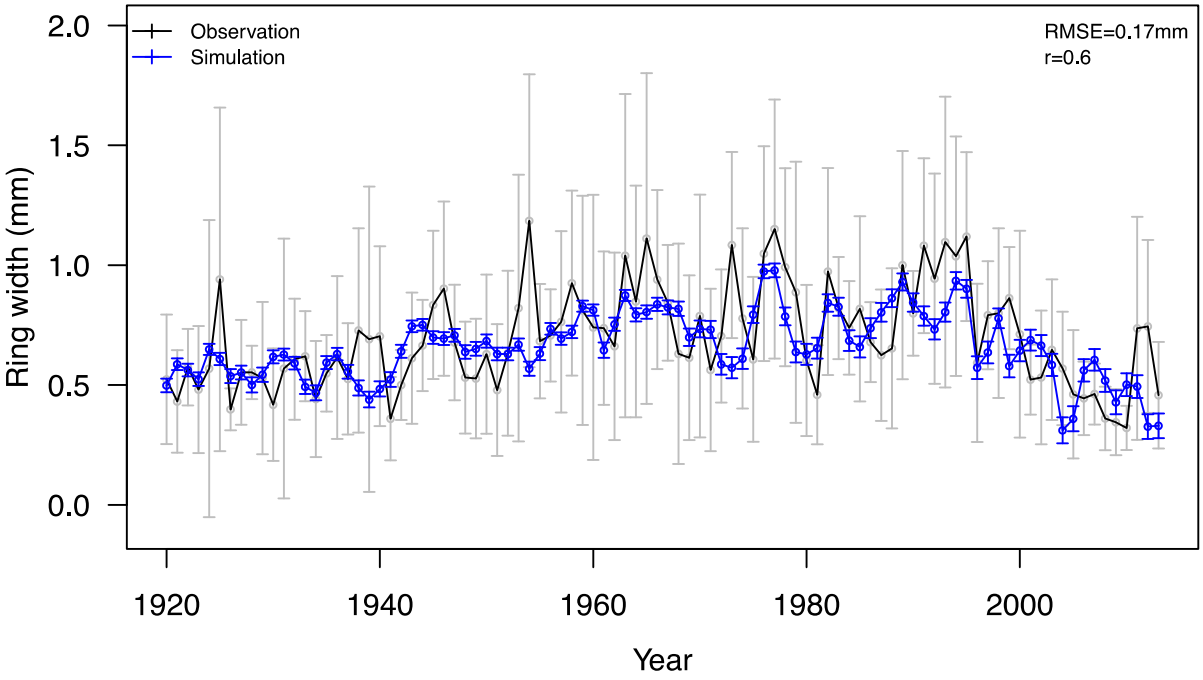

777

778 Figure 5. Simulation of radial growth in response to changing climate and observed [CO_2],
779 allowing for the effect of changing allocation to fine roots. The black line is the mean of the
780 observations, and the grey bars are the standard deviation (SD) among the ten individual
781 trees sampled. The blue line and bars are the mean and standard deviation for the ten
782 simulated individual trees.

783